Transport barriers to self-propelled particles in fluid flows: Supplemental Material

Simon A. Berman, John Buggeln, David Brantley, Kevin A. Mitchell, Thomas H. Solomon

1 Experimental methods

1.1 Incubation protocols

For the tumbling, GFP bacteria (1A1266), a scraping from a sample frozen at $-80°$C is used to inoculate 50 mL of LB broth. This broth is incubated overnight at 37°C (with shaking), reinoculated in the morning in fresh LB broth, incubated for 3 hours, and then diluted to an optical density $(\mathrm{OD})_{600} \sim 0.02$. (A shorter incubation time results in a smaller optical density without need for dilution, but the bacteria rely on quorum sensing to turn on their swimming, so that approach results in most of the bacteria remaining sessile.)

The smooth-swimming bacteria (OI4139) are incubated in CAP medium [1]. The following stock solutions are used: (a) a salt solution, composed of 6.80 g KH_2PO_4, 8.70 g K_2HPO_4, 0.240 g $MgCl_2$, 0.132 g NH_4SO_4, and 0.00125 g $MnCl_2$, mixed in 1.0 L of distilled water and autoclaved (a precipitate forms during autoclaving, which is filtered out later in the process); (b) 1.00 g of $CaCl_2$ in 50 ml of water; (c) 0.050 g each of histidine, methionine, and tryptophan in 10 ml of water; (d) 1.80 g of sorbitol in 10 ml of water; (e) 10.0 g of tryptone and 5.0 g NaCl in 1 L of water (or 15.0 g of "tryptone water" powder in 1 L of water); (f) 1.20 g of IPTG in 20 ml of water; and (g) 2.5 ml of glycerin in 47.5 ml of water. To prepare incubation media, 50 ml of the salt solution is combined with 0.23 ml of the $CaCl_2$ solution, 0.15 ml of the HMT solution, 0.50 ml each of the sorbitol and Tryptone broth solutions, and 0.20 ml of IPTG solution. (For the overnight incubations, we often double the tryptone broth concentration.) This mixture is then filter-sterilized and divided into ten 5-ml samples, each in a 15-ml capacity centrifuge tube.

Scrapings of smooth-swimming bacteria (OI4139) from frozen stock are used to inoculate one of the 5-ml CAP solutions, which is then incubated overnight at 37°C (with shaking), reinoculated in the morning into a fresh CAP solution, incubated for 4 hours, injected with 0.050 ml (2 drops) of the glycerol solution, incubated for an additional 15 minutes, and then diluted to an optical density $(\mathrm{OD})_{600} \sim 0.03$.

1.2 Tracking and three-dimensional (3D) effects

Trajectories for both passive microspheres and bacteria are extracted using standard particle tracking algorithms [2]. The swimming speed v_0 and the orientation θ of each bacterium are determined by subtracting the hyperbolic flow velocity from the velocity of the trajectory: $v_0\hat{\mathbf{n}} = \dot{\mathbf{r}} - \mathbf{u}(\mathbf{r})$ [3, 4].

A small fraction of the smooth-swimming bacteria still tumble after these procedures. We identify those bacteria from the trajectories by large, abrupt changes in orientation angle θ; these tumblers are discarded from our analysis of the smooth-swimming bacteria.

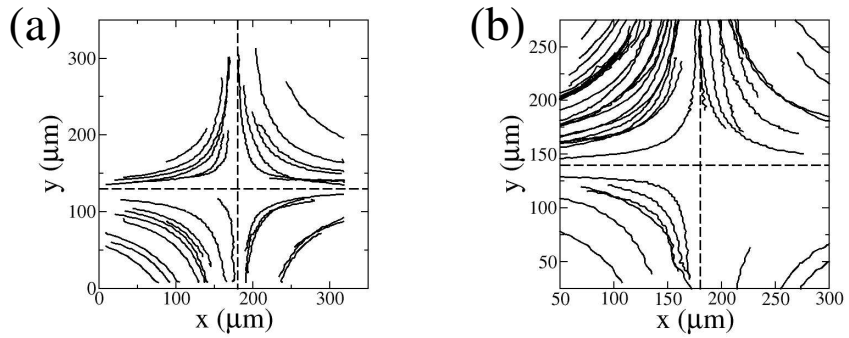

Figure S1: Trajectories of sessile bacteria in a flow with $A = 0.44$ s^{-1}. (a) Sessile bacteria in the same experiment as shown in Fig. 2a. (b) Sessile bacteria in the same experiment as shown in Fig. 4a. The dashed lines show the same passive manifolds as in Figs. 2 and 4.

The analysis treats the bacteria as though swimming in a two-dimensional (2D) plane. However, even though the flow itself is predominantly 2D, the bacteria can swim with velocity components perpendicular to the focal plane of the microscope. With the 40X objective, the focal plane of the microscope is able to image bacteria over a thickness of approximately 20 - 30 μm for the smooth swimming bacteria using diascopic microscopy, and approximately 50 - 60 μm for the fluorescent (tumbling) bacteria imaged under epi-fluorescence illumination. Given typical tracking times and swimming speeds, the smooth swimming bacteria tracked in Fig. 2 likely have swimming orientations that are within 20° of the 2D focal plane. Of course, the tumbling bacteria in Fig. 4 may have orientations at larger angles relative to the focal plane, especially right after a tumble event. In those cases, the bacteria would swim out of the focal region quickly, so those larger angles are presumably near the ends of the plotted trajectories.

Ultimately, the 2D trajectories plotted and analyzed are 2D projections of the full 3D motion. The true swimming speed of the bacteria may be larger than that reported (which is based on the 2D projection), but the theory accurately captures the behavior of the 2D projections of the trajectories, based on the swimming speeds of the projections.

2 Additional experimental data

2.1 Passive (Sessile) bacteria

For each of the experimental runs reported, there are bacteria that are sessile (non-motile) or that swim with sufficiently small speeds as to behave as though sessile. We plot the trajectories of these sessile bacteria in Fig. S1. For these non-swimming bacteria, the passive manifolds are the barriers. This verifies that the crossing of the passive manifold seen in Figs. 2 and 4 is due to the swimming of the organisms.

2.2 Motile bacteria in a slower flow

The data in Figs. 2 and 4 cover a range of v_0/A of over a factor of two in each case, since the bacteria swim with a range of swimming speeds. But the theory works equally well if v_0/A is varied by changing the flow speed parameter A. Figure S2 shows data similar to that in Figs. 2 and 4, but for a flow rate less than half as strong. Once again, every trajectory

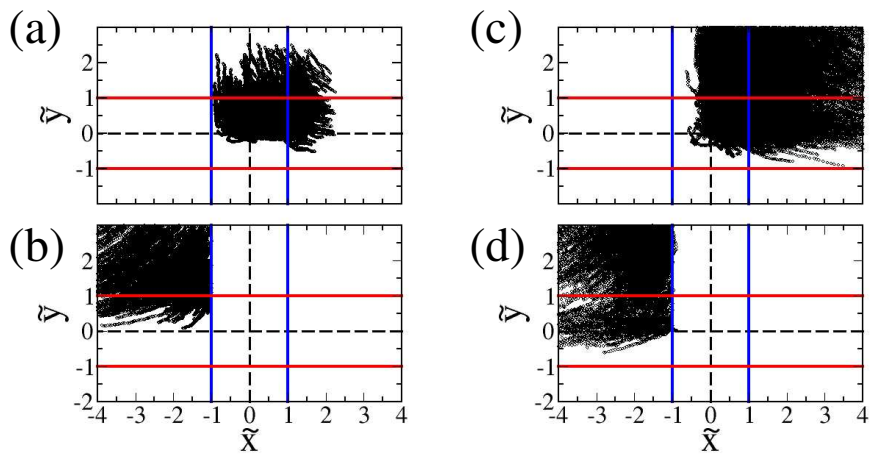

Figure S2: Scaled bacteria trajectories ($\widetilde{x} = (A/v_0)x$) for a hyperbolic flow with $A = 0.19$ s^{-1}. The left two panels show results for smooth-swimming bacteria: (a) rectified plot with every trajectory that leaves to the right; and (b) rectified plot with every trajectory that enters with non-dimensional $\widetilde{x} < -1.0$. The right two panels show similar data for tumbling bacteria. Passive manifolds are shown with dashed lines and the theoretically predicted SwIM edges are shown with red and blue lines.

that ends up leaving toward the right enters to the right of the left SwIM edge (Figs. S2a and S2c). And every trajectory that enters to the left of the left SwIM edge exits to the left (Figs. S2b and S2d).

There is a depletion zone next to the SwIM edge for the tumbling bacteria (Fig. S2c), which is also seen for the higher flow rate (Fig. 4d). This depletion region exists because tumbling bacteria that begin on the right of the SwIM edge can tumble and swim left across this one-way barrier, but they can't cross back once outside the SwIM edge, since it blocks inward-swimming bacteria.

3 Burning invariant manifolds (BIMs)

Here we provide background information on burning invariant manifold (BIM) theory [5, 6, 7]. Initially, this theory was developed to describe barriers to the propagation of chemical reaction fronts in a 2D fluid flow $\mathbf{u}(\mathbf{r})$. Fronts are represented by parametrized curves $(\mathbf{r}(\lambda), \theta(\lambda))$, where $\mathbf{r}$ is the 2D position and θ is the angle of the normal to the front $\hat{\mathbf{n}}(\lambda) = \cos\theta(\lambda)\hat{\mathbf{x}} + \sin\theta(\lambda)\hat{\mathbf{y}}$, which satisfy

$$\frac{d\mathbf{r}}{d\lambda} \cdot \hat{\mathbf{n}}(\lambda) = 0. \tag{S1}$$

Equation (S1) is known as the front-compatibility criterion [6]. A point on the front, i.e. a front element $(\mathbf{r}, \theta)$, evolves in time according to the equations

$$\dot{\mathbf{r}} = \mathbf{u}(\mathbf{r}) + v_0\hat{\mathbf{n}}, \tag{S2a}$$

$$\dot{\theta} = \frac{\omega_z}{2} - \hat{\mathbf{n}}_\perp \cdot \mathbf{E}\hat{\mathbf{n}}, \tag{S2b}$$

where v_0 is the local front-propagation speed and ω_z and $\mathbf{E}$ are the vorticity and rate-of-strain tensor, respectively. Equation (S2) is simply Eq. (1) with $\alpha = -1$; hence, front-

element dynamics is equivalent to the dynamics of a rod-shaped swimmer that swims perpendicular to its axis [6].

BIMs are defined as the one-dimensional invariant manifolds of the fixed points of Eq. (S2). Because Eq. (S2) assumes the flow has no explicit time-dependence, BIMs are solutions of Eq. (S2) that asymptotically approach a fixed point forwards or backwards in time. They are special cases of swimming invariant manifolds (SwIMs): they are the one-dimensional SwIMs of the swimming fixed points (SFPs) of $\alpha = -1$ swimmers. For example, for the hyperbolic flow [Eq. (2)], the SFPs $\mathbf{q}_{\pm}^{\text{in}}$ have one stable and two unstable directions when $\alpha = -1$. Thus, their one-dimensional stable manifolds are BIMs (blue curves in Fig. 1b). Conversely, the SFPs $\mathbf{q}_{\pm}^{\text{out}}$ have one unstable and two stable directions when $\alpha = -1$. Thus, their one-dimensional unstable manifolds are BIMs (red curves in Fig. 1b). For the vortex flow, the SFPs surrounding the hyperbolic fixed points also possess BIMs, i.e. one-dimensional invariant manifolds when $\alpha = -1$, so long as v_0 is not too large [8].

BIMs belong to a special family of solutions of Eq. (S2) for which the front element trajectories are themselves fronts. These special solutions, called sliding fronts [7], are defined as those satisfying Eq. (S1) with $\lambda \to t$. Explicitly, we have

$$\dot{\mathbf{r}}(t) \cdot \hat{\mathbf{n}}(t) = \mathbf{u}(\mathbf{r}(t)) \cdot \hat{\mathbf{n}}(t) + v_0 = 0 \tag{S3}$$

all along the trajectory, which is known as the sliding-front condition. It follows from direct calculation that if Eq. (S3) is satisfied at some initial time, then it is satisfied for all time [7]. In particular, this is true for BIMs, and hence the BIM trajectory $(\mathbf{r}(t), \theta(t))$ is itself a front. By virtue of Eq. (S3), BIMs satisfy the inequality Eq. (3). Therefore, they are one-way barriers to swimmers, regardless of α or any noise in the orientation.

4 Vortex flow simulations

To simulate the swimmer dynamics in the vortex flow, we investigate the trajectories of Eq. (1) with $\mathbf{u} = (U \sin(2\pi x/L)\cos(2\pi y/L), -U\cos(2\pi x/L)\sin(2\pi y/L))$, where L is the flow length scale and U is the maximum flow speed. Thus, the equations of motion are

$$\dot{x} = U \sin\left(\frac{2\pi x}{L}\right)\cos\left(\frac{2\pi y}{L}\right) + v_0 \cos\theta, \tag{S4a}$$

$$\dot{y} = -U \cos\left(\frac{2\pi x}{L}\right)\sin\left(\frac{2\pi y}{L}\right) + v_0 \sin\theta, \tag{S4b}$$

$$\dot{\theta} = \frac{2\pi U}{L}\left[\sin\left(\frac{2\pi x}{L}\right)\sin\left(\frac{2\pi y}{L}\right) - \alpha\cos\left(\frac{2\pi x}{L}\right)\cos\left(\frac{2\pi y}{L}\right)\sin(2\theta)\right] + \xi(t). \tag{S4c}$$

Here, we have added a Gaussian white-noise term $\xi(t)$ to Eq. (S4c) to model rotational diffusion. The noise is zero-mean and delta-correlated with rotational diffusivity D_r:

$$\langle \xi(t) \rangle = 0, \tag{S5a}$$

$$\langle \xi(t)\xi(t') \rangle = 2D_r\delta(t - t'). \tag{S5b}$$

Non-dimensionalizing Eq. (S4) with coordinates $\widetilde{\mathbf{r}} = \mathbf{r}/L$ and $\widetilde{t} = tU/L$, we find that the relevant system parameters are the dimensionless quantities v_0/U, D_rL/U, and α. All calculations in the main text are for $\alpha = 1$ swimmers.

Event	Symbol
Moving down through $\widetilde{y} = 0.25$	1
Moving right through $\widetilde{x} = 0$	2
Moving down through $\widetilde{y} = 0$	3
Moving left through $\widetilde{x} = -0.25$	4
Moving left through $\widetilde{x} = -0.5$	5
Moving up through $\widetilde{y} = 0.5$	6

Table S1: Symbols assigned to swimmer trajectories for certain events.

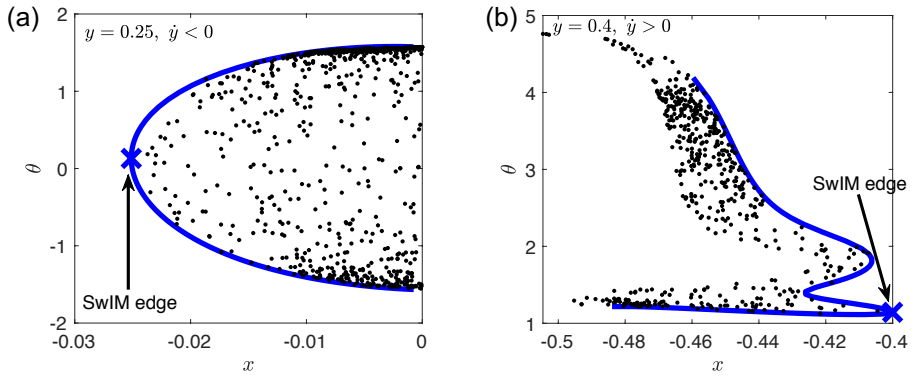

Figure S3: Cross sections of stable SwIM (blue curves) at $\widetilde{y} = 0.25$ [$\dot{\widetilde{y}} < 0$, (a)] and $\widetilde{y} = 0.4$ [$\dot{\widetilde{y}} > 0$, (b)]. The black dots show the intersections of the "12" swimmer trajectories, which eventually exit right, with the surface of section; $D_r = 0$.

We select N random swimmer initial conditions and integrate them from $\widetilde{t} = 0$ to $\widetilde{t} = 3$. The initial positions are uniformly randomly distributed inside a single vortex cell with $-0.5 < \widetilde{x} < 0$ and $0 < \widetilde{y} < 0.5$ but outside the grey square illustrated in Fig. 5, defined by $-0.25 \leq \widetilde{x} \leq 0$ and $0 \leq \widetilde{y} \leq 0.25$, and the initial orientations are also uniformly randomly distributed in the full range $\theta \in [0, 2\pi]$. For each trajectory, we record certain events related to entering or leaving the grey square or the vortex cell using a numeric symbol, as detailed in Table S1. Clearly, a swimmer must register one of the symbols "2," "3," "5," or "6" when it exits the vortex cell. For a swimmer that registers a symbol "1" immediately followed by "2," "3," or "4," it is assumed the swimmer entered the square through the top side and subsequently exited via one of the remaining sides. For instance, the label "12" means the swimmer enters the square from the upper side, exits on the right side, and never subsequently returns to the square; the label "1413" means the swimmer completes a full revolution around the vortex center, returns to the square and exits on the lower side.

In Fig. 5, we plot only the initial positions of swimmers whose trajectory labels begin with "12," from a simulation with $N \approx 2 \times 10^4$. In Supplemental Movie S1, we provide an animation of the calculation with $D_r = 0$ leading to Fig. 5a, i.e. for perfect smooth swimmers (with $N \approx 10^3$ for clarity). Swimmers whose labels begin with "12" are the large, green dots, while the remaining swimmers whose first symbols are "1" are the small, grey dots. The arrows indicate instantaneous swimming directions. All other trajectories are discarded from the animation for clarity. In Supplemental Movie S2, we provide an animation of the analogous calculation with $D_r L/U = 0.86$ leading to Fig. 5b.

For the vortex flow (S4), we compute the SwIM edge as follows. Equations (S4) have an

SFP at $\mathbf{q} = (-\sin^{-1}(v_0/U)/(2\pi), 0, 0)$ in rescaled units, which is a saddle with two stable directions and one unstable [8]. We compute the 2D stable SwIM by integrating trajectories initialized near the SFP in the 2D stable subspace backwards in time. Cross-sections of part of the 2D SwIM at different $\widetilde{y}$ positions away from the SFP are shown in Fig. S3. We locate the SwIM edge at every angle ϕ relative to the center of the vortex as the point on the SwIM which is closest to the vortex center at that ϕ. These points are indicated in Fig. S3 by the arrows. Figure S3 shows that all swimmers that exit right remain on the outer side of the SwIM (relative to the vortex center). Hence, in $\widetilde{x}\widetilde{y}$ space, their trajectories are bounded by the SwIM edge.

References

[1] R. Rusconi, J. S. Guasto, and R. Stocker. Bacterial transport suppressed by fluid shear. *Nat. Phys.* **10**, 212 (2014).

[2] J. C. Crocker and D. G. Grier. Methods of digital video microscopy for colloidal studies. *J. Colloid Interface Sci.* **179**, 298 (1996).

[3] M. T. Barry, R. Rusconi, J. S. Guasto, and R. Stocker. Shear-induced orientational dynamics and spatial heterogeneity in suspensions of motile phytoplankton. *J. R. Soc. Interface* **12**, 20150791 (2015).

[4] G. Junot, N. Figueroa-Morales, T. Darnige, A. Lindner, R. Soto, H. Auradou, and E. Clément. Swimming bacteria in Poiseuille flow: The quest for active Bretherton-Jeffery trajectories. *EPL* **126**, 44003 (2019).

[5] J. R. Mahoney, D. Bargteil, M. Kingsbury, K. A. Mitchell, and T. H. Solomon. Invariant barriers to reactive front propagation in fluid flows. *EPL* **98**, 4405 (2012).

[6] K. A. Mitchell and J. R. Mahoney. Invariant manifolds and the geometry of front propagation in fluid flows. *Chaos* **22**, 037104 (2012).

[7] J. R. Mahoney, J. Li, C. Boyer, T. H. Solomon, and K. A. Mitchell. Frozen reaction fronts in steady flows: A burning-invariant-manifold perspective. *Phys. Rev. E* **92**, 063005 (2015).

[8] S. A Berman and K. A Mitchell. Trapping of swimmers in a vortex lattice. *Chaos* **30**, 063121 (2020).